Cell Death & Differentiation (2020) 27:1225–1242
https://doi.org/10.1038/s41418-019-0425-3

Cell Death & Differentiation

ARTICLE

LIN28B increases neural crest cell migration and leads to transformation of trunk sympathoadrenal precursors

Diana Corallo[1] · Michael Donadon[1] · Marcella Pantile[1] · Viktoryia Sidarovich[2] · Simona Cocchi[2] · Michela Ori[3] · Miriam De Sarlo[3] · Simona Candiani[4] · Chiara Frasson[5] · Martin Distel[6] · Alessandro Quattrone[2] · Carlo Zanon[5] · Giuseppe Basso[7] · Gian Paolo Tonini[1] · Sanja Aveic[1,8]

Received: 7 March 2019 / Revised: 4 September 2019 / Accepted: 12 September 2019 / Published online: 10 October 2019

Abstract

The RNA-binding protein LIN28B regulates developmental timing and determines stem cell identity by suppressing the *let-7* family of microRNAs. Postembryonic reactivation of *LIN28B* impairs cell commitment to differentiation, prompting their transformation. In this study, we assessed the extent to which ectopic *lin28b* expression modulates the physiological behavior of neural crest cells (NCC) and governs their transformation in the trunk region of developing embryos. We provide evidence that the overexpression of *lin28b* inhibits sympathoadrenal cell differentiation and accelerates NCC migration in two vertebrate models, *Xenopus leavis* and *Danio rerio*. Our results highlight the relevance of *ITGA5* and *ITGA6* in the LIN28B-dependent regulation of the invasive motility of tumor cells. The results also establish that *LIN28B* overexpression supports neuroblastoma onset and the metastatic potential of malignant cells through *let-7a*-dependent and *let-7a*-independent mechanisms.

Edited by E. Baehrecke

Supplementary information The online version of this article (https://doi.org/10.1038/s41418-019-0425-3) contains supplementary material, which is available to authorized users.

✉ Diana Corallo
d.corallo@irpcds.org

✉ Sanja Aveic
s.aveic@irpcds.org

[1] Neuroblastoma Laboratory, Fondazione Istituto di Ricerca Pediatrica Città della Speranza, Padova, Italy

[2] Department of Cellular, Computational and Integrative Biology (CIBIO), University of Trento, Trento, Italy

[3] Unit of Cell and Developmental Biology, Department of Biology, University of Pisa, Pisa, Italy

[4] Department of Earth, Environmental and Life Sciences (DISTAV), University of Genoa, Genova, Italy

[5] Fondazione Istituto di Ricerca Pediatrica Città della Speranza, Padova, Italy

[6] Innovative Cancer Models, Children's Cancer Research Institute (CCRI), Wien, Austria

[7] Department of Women and Child Health, Haematology-Oncology Clinic, University of Padua, Padova, Italy

[8] Department of Dental Materials and Biomaterials Research, RWTH Aachen University Hospital, Aachen, Germany

Introduction

Neural crest cells (NCC) undergo substantial modifications in their morphology and function during embryogenesis. Their highly migratory and invasive nature allows them to reach distant body districts, whereas their pluripotency assures the specification of several cell lineages, including peripheral neurons and the adrenal medulla [1, 2]. The initial migratory wave of NCC is activated by the epithelial-to-mesenchymal transition (EMT). The morphological changes triggered by EMT sustain cell migration from the neural tube, invasion of the surrounding tissues, and spatial progression toward the peripheral sites, where cells differentiate and unfold their intrinsic features [3]. Several NCC characteristics, such as motility, polarity, invasiveness, and plasticity, are largely shared by a number of highly metastatic tumors, including colon [4], breast [5], esophagus [6], and neuroblastoma [7] tumors. Neuroblastoma is an embryonal malignancy responsible for ~15% of cancer-related deaths during childhood [8]. It originates from the transformed sympathoadrenal cell precursors deriving from trunk NCC [9] and is characterized by vast clinical, genetic, and biological heterogeneity [10]. About half of patients with neuroblastoma are stratified as high-risk (HR), having an overall survival rate of <40% despite intensive

multimodal therapy [11]. The main feature of HR patients with neuroblastoma is the prevalence of metastases at disease onset. The metastases to the liver, the bone marrow, the bone, or lymph nodes are found in ~50% of HR patients. Like other pediatric cancers, neuroblastoma shows a low frequency of somatic mutations although alterations in several genes, including *LIN28B*, have been associated with this malignancy [12].

The RNA-binding proteins LIN28A/LIN28B were initially identified as important regulators of developmental timing [13]. By inhibiting *let-7* microRNA biogenesis and through direct binding of the target RNAs, LIN28 regulates numerous cellular activities that are essential for embryogenesis [14], but it shows protumorigenic features if maintained beyond the physiologically defined timeframe [15, 16]. In neuroblastoma, the protumorigenic function of *LIN28B* has been attributed to either gene amplification or overexpression [7]. However, the lack of experimental models, in which modulated levels of *LIN28B* can be studied during early developmental phases, limits the possibility for a comprehensive investigation of the mechanisms that sustain NCC transformation.

In this study, we assessed the role of the ectopically expressed zebrafish *lin28b* gene in regulating trunk NCC migration and differentiation toward the sympathoadrenal lineage. In two vertebrate models, zebrafish (*Danio rerio*) and Xenopus (*Xenopus leavis*), we examined how the overexpression of *lin28b* affected the migration of trunk NCC during early embryonic development. We then analyzed whether *lin28b* determined the differentiation of NCC toward noradrenergic lineage. In vivo, a stable overexpression of the human *LIN28B* gene driven by the *dβh* promoter was adopted to evaluate the probability of neuroblastoma onset. In the tumor cells, we focused on evaluating the effects of the prolonged overexpression of *LIN28B* on cell motility and dissemination in vitro and in the in vivo xenograft model. Finally, we established the relevance of integrin-dependent signaling in the regulation of neuroblastoma cell migration upon *LIN28B* overexpression.

Results

Lin28b overexpression impairs the differentiation of sympathoadrenal precursor cells

To estimate the effects of *lin28b* overexpression during embryonic development, we injected capped *lin28b* mRNA into 1–2-cell stage zebrafish embryos. We then assessed the ectopic expression of the corresponding transcript and protein at different developmental stages (Fig. S1A) compared with the control (*ctrl*) embryos, injected with either the mCherry or the GFP mRNAs (Fig. S1B). Wild-type uninjected embryos were used as a blank control for fluorescence screening, and as a reference sample for the evaluation of Lin28b protein levels in the immunoblot assay (Fig. S1B). Of note, the injected fish showed no overt macroscopic phenotypes or developmental failures (Fig. S1C). We then verified the functionality of Lin28b by observing a significant reduction of the *let-7a* expression in *lin28b* embryos (Fig. S1D). To test if Lin28b affected the development of sympathoadrenal neurons, we analyzed the expression of tyrosine hydroxylase (*th*) and dopamine β-hydroxylase (*dβh*) as hallmarks of NCC differentiation toward the sympathoadrenal lineage. The ectopic expression of *lin28b* at early stages of development led to a marked reduction of both *dβh* and *th* mRNAs in the superior cervical ganglia (SCG) as compared with GFP-injected controls (Fig. 1a). Moreover, TH protein levels also significantly decreased upon *lin28b* overexpression (Fig. 1b). In addition, *lin28b*-injected embryos expressed lower levels of the SCG marker *zash1a* (Fig. 1c), a transcription factor required for early sympathoadrenal cell specification [17]. These findings imply the involvement of *lin28b* overexpression in the loss of prodifferentiating signaling in sympathoadrenal cells already at early stages of embryonic development. Then, to verify the evolutionary conservation of Lin28b function in the tetrapods, we performed transient gain-of-function experiments on the Xenopus embryos. In this model, it is possible to specifically target the central nervous system and NCC without affecting the development of other tissues [18]. We therefore injected *lin28b* mRNA into one dorsal blastomere at the four-cell stage (Fig. 1d, left panel) along with GFP mRNA in order to select and further analyze only embryos overexpressing *lin28b* in the developing central nervous system. Comparable with the effects observed previously in the zebrafish, the injected *lin28b* mRNA caused a significant reduction of the sympathoadrenal marker *reptin* in the Xenopus embryos (Fig. 1d, right panel). To assure that the observed reduction of sympathoadrenal cells in *lin28b* embryos was not the result of damaged cell proliferation or induced apoptosis, we stained the SCG with either EdU or activated caspase-3/TUNEL, respectively. We found no significant differences in the number of proliferating TH^+ cells in the SCG of injected embryos (Fig. 1e). Similarly, caspase-3 and TUNEL stainings showed no relevant activation of apoptosis in the SCG of *lin28b* larvae (Figs. 1f and S2). These results confirm that *lin28b* overexpression determines the failure of sympathoadrenal progenitor cell differentiation toward their functional counterparts without affecting their proliferation or viability.

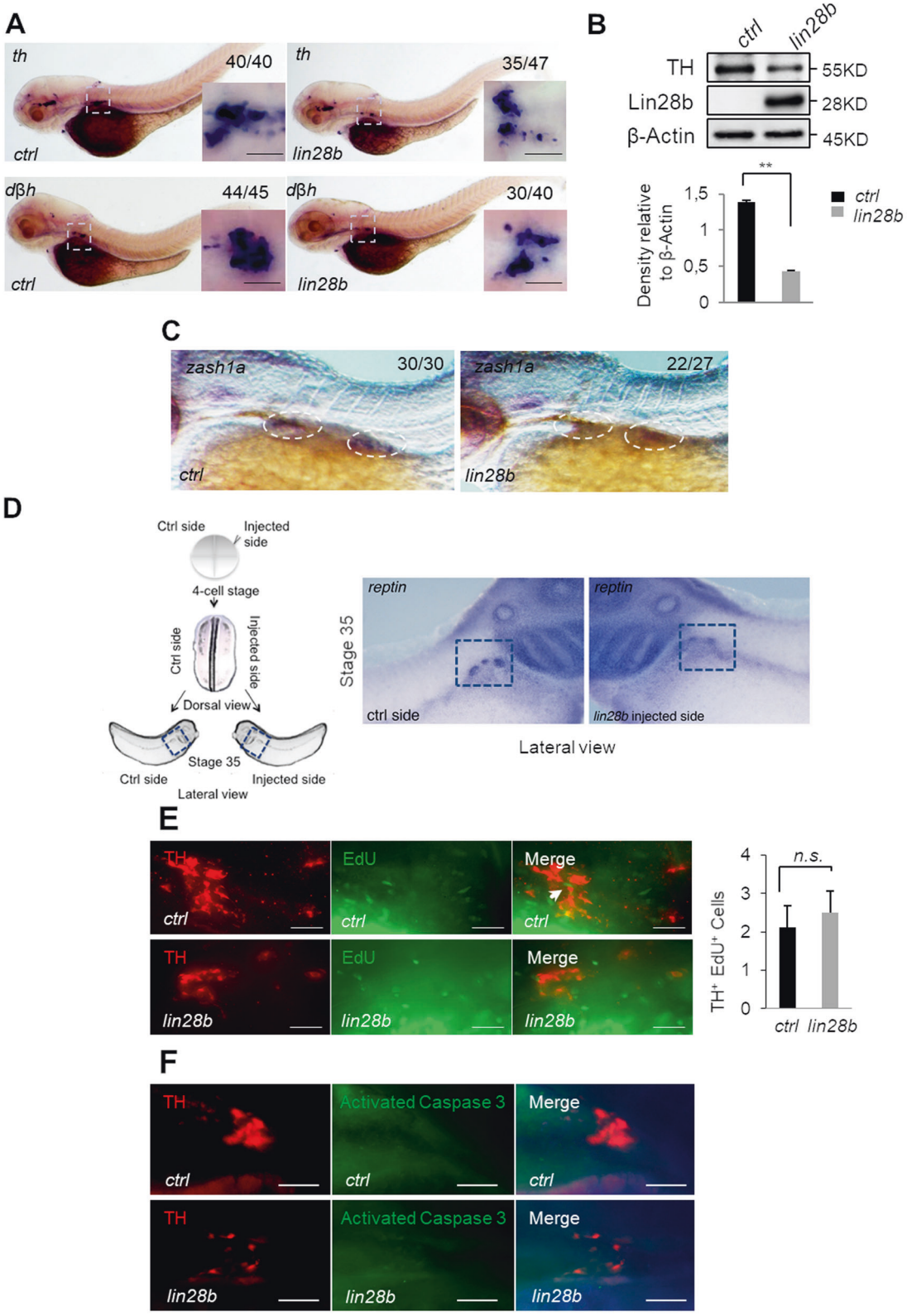
A
th
40/40
ctrl
th
35/47
lin28b
dβh
44/45
ctrl
dβh
30/40
lin28b
B
ctrl
lin28b
TH
55KD
Lin28b
28KD
β-Actin
45KD
**
Density relative to β-Actin
1,5
1
0,5
0
ctrl
lin28b
C
zash1a
30/30
ctrl
zash1a
22/27
lin28b
D
Ctrl side
Injected side
4-cell stage
Ctrl side
Injected side
Dorsal view
Stage 35
Ctrl side
Injected side
Lateral view
Stage 35
reptin
ctrl side
reptin
lin28b injected side
Lateral view
E
TH
ctrl
EdU
ctrl
Merge
ctrl
TH
lin28b
EdU
lin28b
Merge
lin28b
n.s.
TH⁺ EdU⁺ Cells
4
3
2
1
0
ctrl
lin28b
F
TH
ctrl
Activated Caspase 3
ctrl
Merge
ctrl
TH
lin28b
Activated Caspase 3
lin28b
Merge
lin28b

◀ **Fig. 1** *Lin28b* overexpression causes sympathoadrenal cell loss. **a** In situ hybridization for the progenitor markers *dβh* and *th* in the superior cervical ganglia (dashed squares) of the control (*ctrl*) and *lin28b* embryos at 80 hpf. Scale bar: 100 µm. The fraction of embryos displaying the corresponding phenotype is provided in each panel. **b** The western blot analysis of the indicated proteins in the control (*ctrl*) and *lin28b* embryos at 72 hpf. The molecular weights are indicated in kilodaltons (KD). Protein quantification is shown in the lower panel. The error bars represent SEM. $^{**}p < 0.01$. **c** Labeling of *zash1a* mRNA in 72 hpf control (ctrl) and *lin28b* zebrafish embryos. Dashed circles highlight the developing superior cervical ganglia. The fraction of embryos displaying the corresponding phenotype is provided in each panel. **d** The schematic experimental overview is presented on the left side. On the right side, a representative example of a Xenopus embryo (out of 76 embryos analyzed) at stage 35 is shown, indicating the expression of the sympathoadrenal marker *reptin* in the developing adrenal medulla (dashed squares). The lateral view of the *lin28b* injected side (right image) and the uninjected side (ctrl side, left image) of the same embryo is presented. **e** Proliferation of sympathoadrenal progenitors identified by tyrosine hydroxylase (TH) immunolabeling (red) coupled with EdU incorporation (green) in the control (*ctrl*) and *lin28b* embryos at 80 hpf. The quantification is shown in the right panel ($n = 30$ embryos for each group). *n.s.*: $p > 0.05$. Scale bar: 100 µm. **f** The control (*ctrl*) and *lin28b* embryos were stained for activated caspase-3 (green) and TH (red) to detect apoptosis in the superior cervical ganglia at 80 hpf. Scale bar: 100 µm

Impaired cell differentiation promotes neuroblastomagenesis in *LIN28B*-overexpressing zebrafish

To assess whether the *lin28b*-dependent block of peripheral sympathetic neural cell differentiation has protumorigenic effects in fish, we generated the stable transgenic zebrafish line *Tg(dβh: hLIN28B)*, referred to here as *hLIN28B*. For this purpose, human *LIN28B* was overexpressed in the peripheral sympathetic nervous system under the control of the *dβh* promoter. Tumor masses arose in the anterior abdomen of 6-month-old transgenic animals (Fig. 2a) with a 2.4% penetrance. The tumors were found in the interrenal gland, a common site of neuroblastoma onset [19], and consisted of small, undifferentiated, round tumor cells with distinct single nuclei (Fig. 2b). To molecularly characterize and assure the tumor type, we analyzed the expression of several neuroblastoma-specific markers. The tumor cells were strongly immunoreactive for TH (Fig. 2c), indicating their peripheral sympathetic neuronal origin [20]. They were also positive for the HuC/D and the Synaptophysin markers (Fig. 2c), demonstrating that they arose from sympathetic neuroblast precursors, like human neuroblastomas, and not from other NCC derivatives, such as chromaffin cells. Together, these findings evince that the overexpression of human *LIN28B* in the peripheral sympathetic neuronal system of transgenic fish promotes neuroblastomagenesis with a penetrance below 5%, approximately as described for human patients with neuroblastoma.

Overexpressed *lin28b* increases the migratory capacity of trunk NCC

The different number of sympathoadrenal cells composing the SCG between the *lin28b* and control fish reflects the possible involvement of mechanisms regulating either NCC migration or their specification during the early phases of functional commitment. To assess this hypothesis, we used the *Tg(sox10:GFP)* zebrafish transgenic line [21]. In these fish, GFP expression is regulated by the NCC promoter *sox10*, allowing the real-time tracking of the NCC inside developing embryos. Transient overexpression of *lin28b* influenced the migration of trunk NCC, as confirmed by live cell imaging, without influencing the total number of GFP^+ cells (Fig. S3A), their proliferation and viability (Fig. S3B, C). Interestingly, although NCC from both the control and *lin28b* embryos migrated ventrally along somites in narrow stripes as expected (Fig. 3a and Supplementary Video S1A), the NCC overexpressing *lin28b* were first to reach their destination toward the dorsal aorta (Fig. 3a and Supplementary Video S1B). To quantify this phenomenon, we measured the migration distances of NCC labeled with *crestin* riboprobe (Fig. 3b) [22]. The average NCC migration distance was significantly longer in *lin28b* embryos compared with the controls at both monitored time points (Fig. 3c). Importantly, the same behavior was also evident in the Xenopus embryos, where *lin28b*-overexpressing $sox10^+$ NCC cells [23] reached longer distances in the *lin28b* versus the control side of the embryo within the same timeframe (Fig. 3d). Together, these data prove that Lin28b regulates the migration of trunk NCC in different vertebrate models without affecting their proliferation and survival rates. Following, to test how effective Lin28b was in determining the sympathoadrenal lineage specification, we assessed the capability of NCC to form cell lineages other than the sympathoadrenal lineage. First, we analyzed the development of melanocytes originating from trunk NCC [24]. The amount of melanocytes in the yolk sac and the yolk extension was unaffected upon *lin28b* overexpression (Fig. 3e). Moreover, a comparable number of sensory neurons composing the trunk NCC-derived dorsal root ganglia (DRG) was found in both control and *lin28b* larvae (Fig. 3f). Furthermore, the DRG developed in the middle of the single somite boundary, as expected [25]. We then looked at the enteric neurons deriving from vagal NCC [26]. Upon staining with the anti-HuC/D antibody, no significant differences in the number of enteric neurons were found between the control and *lin28b* larvae (Fig. 3g). The finding that *lin28b* embryos lacked trunk NCC-derived sympathoadrenal precursor cells but maintained vagal NCC-derived neurons indicates that Lin28b may play different roles in the designation of specific subpopulations of trunk NCC.

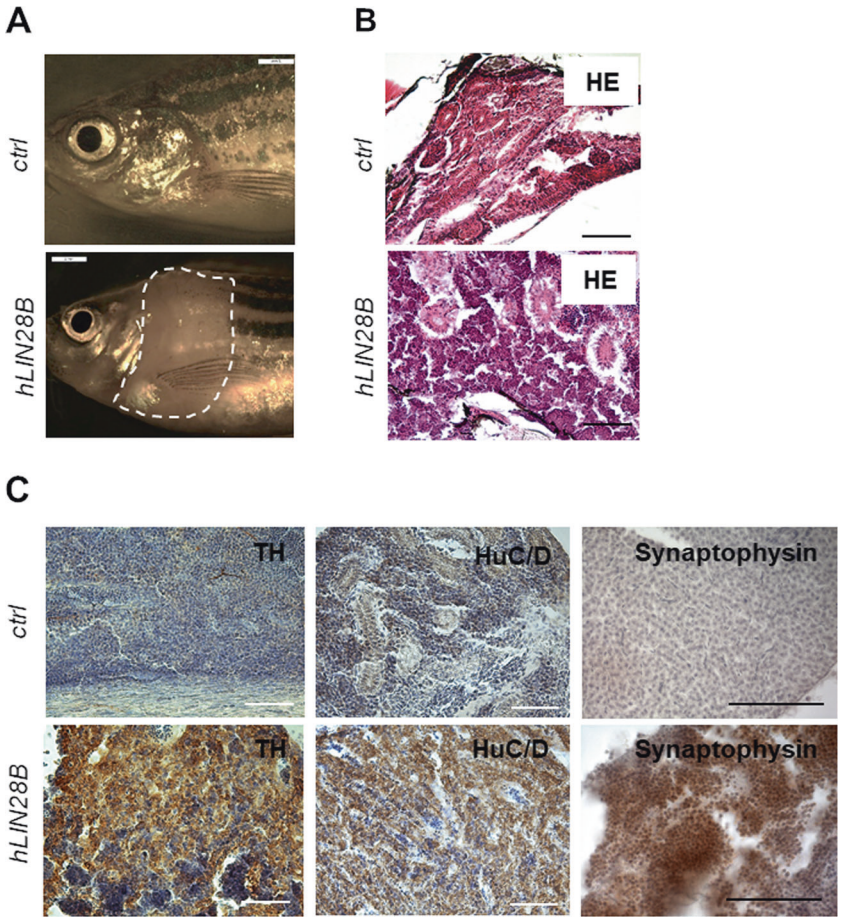

Fig. 2 *LIN28B*-induced neuroblastoma in zebrafish. **a** Macroscopic views of the control (*ctrl*) and *hLIN28B* zebrafish at 6 months of age, showing a tumor mass found in the anterior abdomen (white dashed line). **b** Haematoxylin–Eosin (H&E) staining of the sagittal sections of the tumors in the interrenal gland (IRG) of 6-month-old fish. Scale bar: 100 µm. **c** Immunohistochemical analyses of the sagittal sections of the *Tg(dβh:GFP)* control (*ctrl*) animals and the *hLIN28B* transgenic fish using tyrosine hydroxylase (TH), HuC/D, and Synaptophysin antibodies. Nuclei were counterstained with hematoxylin (purple). Scale bar: 100 µm

Overexpression of *LIN28B* increases the migratory capacity of SH-SY5Y cells

To functionally test the observed in vivo correlations between *lin28b* overexpression and the increased NCC migratory phenotype, we overexpressed *LIN28B* in the neuroblastoma cell line SH-SY5Y under a short-term (48 h) and a long-term (7 days and 14 days) period. *LIN28* is known to be a master regulator of pluripotency in embryonic stem cells [23, 27]. Gene expression analysis indicated that 48 h of *LIN28B* overexpression significantly increased the levels of the stemness-associated genes *Oct4*, *Sox2*, and *Nestin* (Fig. 4a) while preserving colony formation and cell proliferation potentials upon the long-term expression of *LIN28B* in SH-SY5Y cells (SH-SY5Y^{LIN28B}) and the controls (SH-SY5Y^{CTRL}) (Fig. S4A, B). Importantly, while *LIN28B* and *let-7a* expression patterns showed reciprocal expressions after short-term *LIN28B* induction, the *let-7a* levels reverted after prolonged overexpression (Fig. 4b). These findings imply that intervals of *LIN28B* overexpression define molecular mechanisms that can be both *let-7a*-dependent and *let-7a*-independent. Long-term *LIN28B* overexpression provoked consistent changes in cell morphology (Figs. 4c and S4C), which was accompanied by a notable reorganization of cytoskeleton microfilaments (Figs. 4d and S4D). Indeed, SH-SY5Y^{CTRL} cells formed small and stellate-shaped cell clumps, whereas SH-SY5Y^{LIN28B} cells were bigger and cuboidal in shape. Given the role of cytoskeleton reorganization in cell motility [28] and the observed higher migratory rates of NCC upon *lin28b* overexpression in vivo, we analyzed the correlation between these phenomena in vitro. Ectopic *LIN28B* significantly increased the migratory properties of SH-SY5Y^{LIN28B} cells, as revealed by scratch and transwell assays (Fig. 4e, f). A detailed analysis of cell movement using time-lapse imaging showed a sharp increase in total migrated distances (Figs. 4g and S4E; Supplementary Movies S2A and S2B) and in the mean cell velocities of SH-SY5Y^{LIN28B} cells upon 7 days of *LIN28B* induction (Fig. 4h). Notably, motility continued to progress upon *LIN28B* induction for 14 days (Fig. S4F–H; Supplementary Movies S3A and S3B). These results provide further evidence that *LIN28B* overexpression is a determinant factor for defining the migration of neural crest-derived cells both in vitro and in vivo.

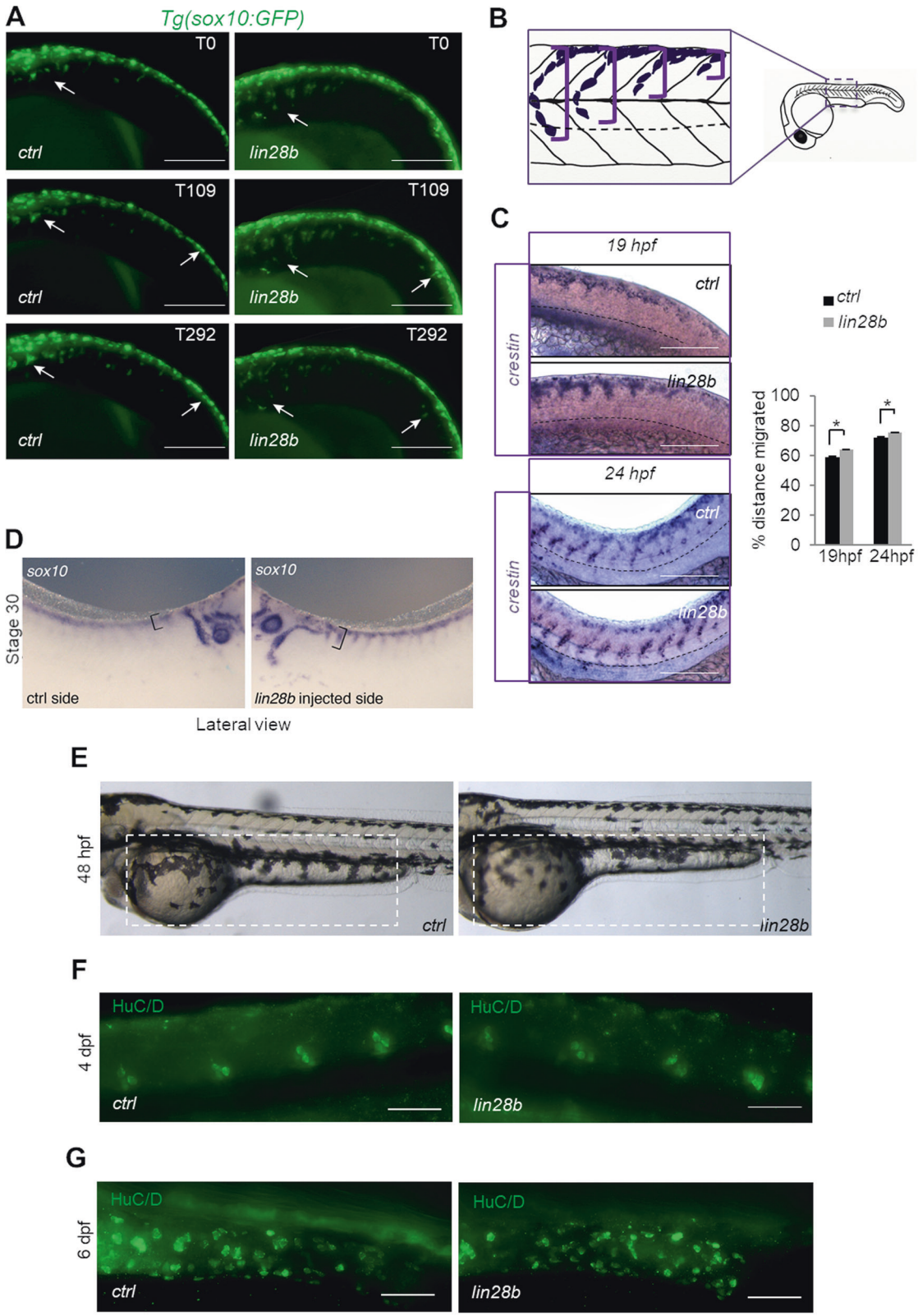
A
Tg(sox10:GFP)
T0
ctrl
lin28b
T109
T292
B
C
19 hpf
24 hpf
crestin
ctrl
lin28b
% distance migrated
19hpf
24hpf
D
Stage 30
sox10
ctrl side
lin28b injected side
Lateral view
E
48 hpf
F
4 dpf
HuC/D
G
6 dpf

◀ **Fig. 3** Lin28b increased the migration speed of trunk NCC. **a** Sequential images of a time-lapse movie in *Tg(sox10:GFP)* embryos showing the motility of NCC in *lin28b* embryos (white arrows) and controls *(ctrl)*. The reported frames were recorded at 19 hpf (T0) after 109 min (T109) and 292 min (T292). Scale bar: 200 µm. **b** The representative scheme depicting the analysis of zebrafish trunk NCC migration. The migrated distance of NCC (purple) toward the dorsal aorta (dotted line) in the same region of the trunk (from somite 8 to somite 12) of embryos injected with the GFP mRNA (*ctrl*) or with *lin28b* mRNA (*lin28b*) has been analyzed. **c** A total of 50 injected embryos per group were stained with the *crestin* riboprobe at 19 hpf (upper panel) and 24 hpf (lower panel), displaying the migration of trunk NCC toward the ventral region of the notochord (dotted black lines). The quantification of the percentage of the migrated distance is shown in the graph. $*p < 0.05$. Scale bar: 100 µm. **d** The trunk *sox10*$^+$ NCC of the uninjected (ctrl; left image) and *lin28b* injected (right image) sides of the Xenopus analyzed at stage 30 (out of the 89 embryos analyzed). A migrated distance of NCC (black square brackets) toward the dorsal aorta is depicted. **e** Imaging of the control (*ctrl*) and *lin28b* embryonic pigment patterns at 48 hpf showed melanocytes populating the yolk sac and the equal yolk extension (dashed squares) between the two groups (the average number of melanocytes in controls = 29 ± 4 and *lin28b* embryos = 28 ± 5, *p-value* = 0.31). **f** The HuC/D antibody staining (green signal) revealed the presence of segmentally arranged dorsal root ganglia in the trunk of both the controls (*ctrl*) and *lin28b* embryos at 4 dpf (the average number of HuC/D$^+$ cells in controls = 20 ± 2 and *lin28b* embryos = 22 ± 3, *p-value* = 0.2). For individual cell counts composing the zebrafish dorsal root ganglia (DRG), the five most caudal DRG labeled with the HuC/D antibody were counted for each condition ($n = 30$ embryos per group). **g** The number of HuC/D-positive enteric neurons (green-positive nuclei) remained comparable between the *lin28b* embryos compared with the control (*ctrl*) siblings at 6 dpf (the average number of HuC/D$^+$ cells in controls = 36 ± 4 and *lin28b* embryos = 33 ± 5, *p-value* = 0.4. $n = 30$ embryos per group). Scale bar: 100 µm

LIN28B promotes the invasive motility of neuroblastoma cells

The core feature of highly aggressive tumors is their metastatic potential determined by enhanced cell migration and invasion abilities. Both features are also mandatory for the proper function of NCC during embryogenesis. To investigate whether LIN28B may sustain cell invasiveness, we analyzed the capacity of SH-SY5Y^{LIN28B} cells to infiltrate the matrigel-coated Boyden chambers (Fig. 5a, upper panel). This assay confirmed an increased capacity of SH-SY5Y^{LIN28B} cells to invade the basement membrane following a chemo-attractant gradient when compared with the control SH-SY5Y^{CTRL} counterpart (Fig. 5a, graph bars). To confirm these findings in vivo, we injected either SH-SY5Y^{LIN28B} or SH-SY5Y^{CTRL} cells into the duct of Cuvier of *Tg(fli1:GFP)* zebrafish embryos with blood vessels marked in green. While SH-SY5Y^{LIN28B} cells showed a rapid spread inside the vessels and clear distribution throughout the trunk of the embryos 1-day post injection, SH-SY5Y^{CTRL} cells did not disseminate in the same way (Fig. 5b). This proinvasive phenotype was sustained by EMT induction, as SH-SY5Y^{LIN28B} cells expressed significantly higher levels of the mesenchymal markers N-cadherin, Snail, Twist1, and Slug compared with the control cells upon long-term *LIN28B* induction (Figs. 5c and S5A). Consistently, the levels of *N-cadherin, Snail, Twist1*, and *Slug* genes were also significantly upregulated after *LIN28B* ectopic expression (Fig. 5d). These findings explained the previously observed changes in SH-SY5Y^{LIN28B} cell morphology (Fig. 4d) that aligned well with the mesenchymal-like phenotype. In line with these outcomes, the overexpression of *lin28b* in the zebrafish embryos led to a global activation of EMT (Fig. 5e–g) as well. Taken together, the results imply that LIN28B is sufficient to trigger EMT and to increase the invasive capacities of neural crest-derived neuroblastoma cells.

LIN28B activates integrin-signaling pathways

The migration of trunk NCC during body segmentation and somitogenesis is mediated by their interaction with the extracellular matrix (ECM) components. Integrins are a family of transmembrane receptors required for cell adhesion and their migration [29–31]. To investigate whether the acquired migratory and invasive potentials of *LIN28B*-overexpressing neuroblastoma cells could be attributed to integrin signaling, we evaluated the gene expression patterns of a number of integrins. Out of the nine transcripts analyzed, the most apparent upregulation was found for two integrins, α5-integrin (*ITGA5*) and α6-integrin (*ITGA6*). Both of these showed a substantial induction upon prolonged *LIN28B* overexpression (Fig. 6a). Accordingly, the expression of the corresponding proteins, ITGA5 (CD49e) and ITGA6 (CD49f), was triggered in SH-SY5Y^{LIN28B} cells (Figs. 6b and S5B–D) and confirmed by flow cytometry analyses (Fig. 6c, d). Then, to assess the importance of the two transmembrane proteins in the regulation of SH-SY5Y^{LIN28B} cell motility, we examined their migration upon the addition of antagonizing primary antibodies. Pretreatment with either the blocking antibodies anti-ITGA5 (ITGA5ab) or anti-ITGA6 (ITGA6ab) successfully abolished the migration of *LIN28B*-overexpressing cells (Fig. 6e, f and Supplementary Videos S5–S8). Correspondingly, cell speed was dramatically reduced only in ITGA5ab- and ITGA6ab-treated SH-SY5Y^{LIN28B} cells, suggesting that the previously described promigratory phenotypes were largely hooked up by the two cell-surface integrins in *LIN28B*-overexpressing cells. Because the integrin clustering is essential for the early phases of cell adhesion to the substrate, we next assessed if the observed phenotype was associated with altered focal adhesions' (FAs) formation. While the SH-SY5Y^{CTRL} cells exhibited a diffuse cytosolic distribution of FA adapter proteins Paxillin, focal adhesion kinase (FAK), and Vinculin [32], the SH-SY5Y^{LIN28B} cells possessed these proteins organized on

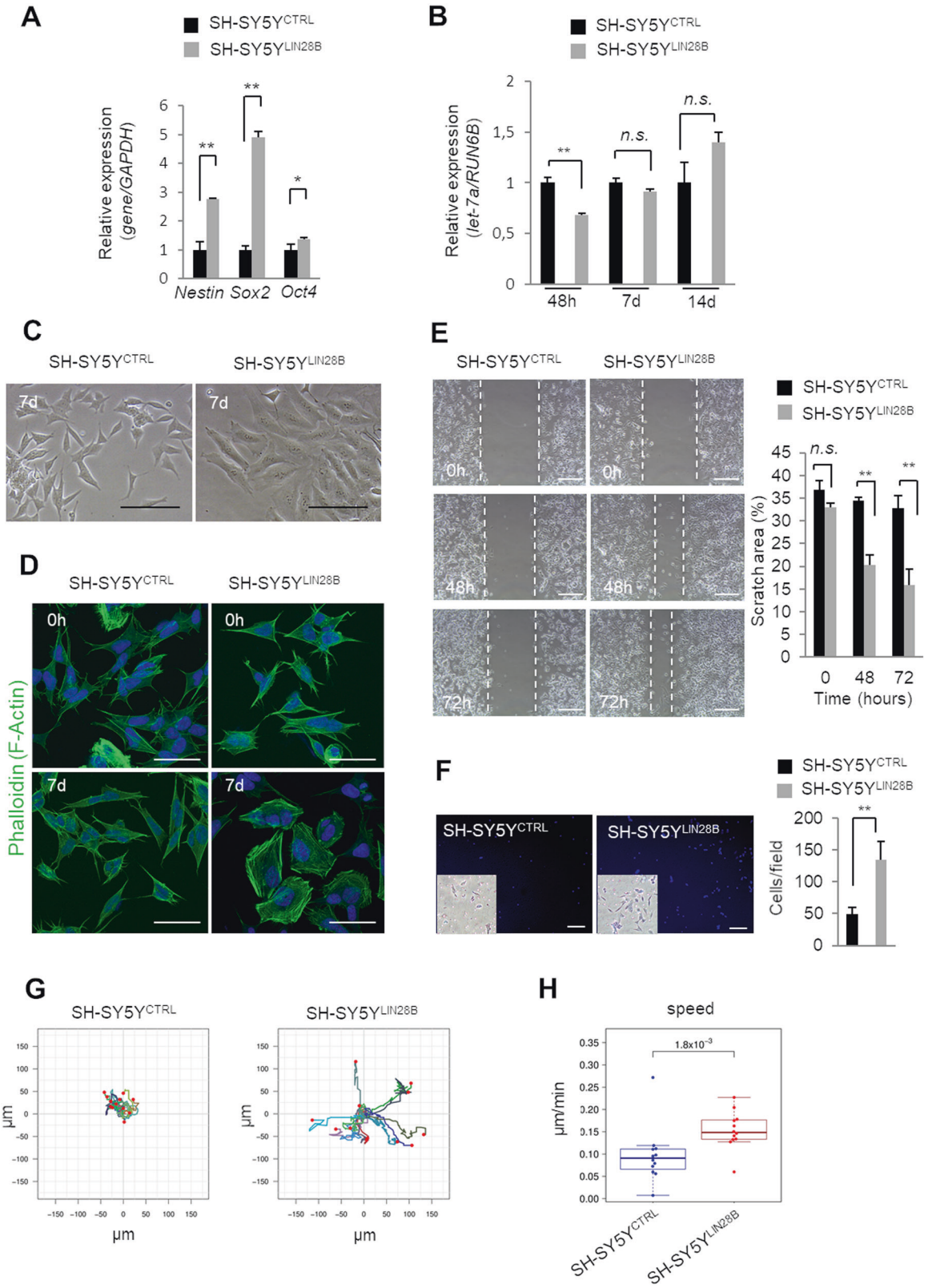

the plasma membrane as punctate, peripheral adhesions (Figs. 7a and S6A). At day 7, these modifications were sustained mainly by the activation of two integrin/FAK-related signaling routes, including PI3K p85/AKT^{Ser473} and Src pathways (Figs. 7b and S6B). Both signaling cascades are important players in regulating the integrin-based cell

◀ **Fig. 4** The Overexpression of *LIN28B* in SH-SY5Y cells potentiates their migratory phenotype. **a** The qPCR analysis showed a significantly increased expression of the stemness markers *Nestin*, *Sox2*, and *Oct4* upon 7 days [d] of *LIN28B* overexpression. The results show the average of three biological replicate experiments. *GAPDH* was used as the internal control. The error bars represent SEM. $^{**}p < 0.01$, $^{*}p < 0.05$. **b** The *let-7a* level was evaluated at several time points upon LIN28B induction (48 hours [h], 7 and 14 d) through qPCR analyses. The results display the mean values of the relative expression ± error bars representing SEM. $^{**}p < 0.01$; *n.s.*: $p > 0.05$. **c** The morphology of the SH-SY5Y^{CTRL} and SH-SY5Y^{LIN28B} cells treated with doxycycline for 7 d. Scale bar: 100 µm. **d** Phalloidin (F-Actin) staining (green) of the SH-SY5Y^{CTRL} and SH-SY5Y^{LIN28B} cells upon 0 h and 7 d of doxycycline treatment. Scale bar: 50 µm. **e** The SH-SY5Y^{CTRL} and SH-SY5Y^{LIN28B} cells were examined for their migratory capacity in a wound healing assay upon 7 d of doxycycline administration. Representative photographs are reported in the left panel. The percentage of wound closure at every time point was calculated relative to the wound width at 0 h (right graph bars). *n.s.*: $p > 0.05$; $^{**}p < 0.01$. Scale bar: 100 µm. **f** The transwell migration assay on SH-SY5Y^{CTRL} and SH-SY5Y^{LIN28B} cells upon 7 d of doxycycline administration. Migrated cells were stained with DAPI (blue) and cristal violet (insets) and counted in following for ten separated fields. $^{**}p < 0.01$. Scale bar: 100 µm. **g** The cell motility tracks of SH-SY5Y^{CTRL} and SH-SY5Y^{LIN28B} cells ($n = 15$ cells tracked) treated with doxycycline for 7 d. The red dots indicate the final cell positions on their path. The distances are presented in µm. **h** The dot plot reports the average cell speed (µm/min) of the SH-SY5Y^{CTRL} and SH-SY5Y^{LIN28B} cells upon 7 d of doxycycline administration. $p = 1.4 \times 10^{-3}$

motility [33, 34]. However, at day 14 only ERK activation was detected (Fig. S6C), implying for a dynamic temporal regulatory switch between multiple signaling proteins in *LIN28B*-overexpressing cells. Taken together, our observations attribute to LIN28B a novel role in orchestrating the integrin-mediated cell spreading and migration.

Discussion

The highly conserved RNA-binding protein LIN28B is expressed in developing tissues and is required for proper embryogenesis [13]. One of the most recognized roles of LIN28B involves the inhibition of the tumor suppressing *let*-7 family of microRNAs [14], contributing to the maintenance of cell pluripotency. The altered expression of *LIN28B* has been reported in various types of human cancer [4, 35, 36] while its role as an oncogene has been confirmed in different mouse models [7, 37]. In neuroblastoma, genomic amplification or overexpression of *LIN28B* are associated with the HR group of patients for whom the widespread metastatic disease is regularly present [7]. Nevertheless, *LIN28B*-driven mechanisms of tumorigenesis are still poorly characterized for neuroblastoma, especially because the onset of this tumor occurs during the early embryonic developmental stages.

In this study, we assessed the in vivo effects of fish *lin28b* overexpression on the NCC compartment. We relied on the zebrafish and Xenopus vertebrate models to demonstrate that the ectopic expression of *lin28b* led to a block in the differentiation of NCC-derived sympathetic progenitor cells without affecting their proliferation or vitality. We showed that Lin28b is required for the commitment of trunk NCC toward the sympathoadrenal cell lineage but is dispensable for the delineation of other NCC derivatives, such as pigmented cells and enteric neurons. This raises the possibility that Lin28b-derived signaling may act in specific NCC subpopulations in which the overexpression of *lin28b* beyond its physiological timeframe is sufficient for the malignant transformation of trunk sympathoadrenal cell precursors and for neuroblastoma's onset. In fact, the transgenic zebrafish model with *dβh*-driven overexpression of human *LIN28B* caused tumors in six-month-old fish. These tumors showed high immunohistochemical similarities with human neuroblastomas and with previously reported neuroblastomas developed in zebrafish [38]. More importantly, the penetrance of LIN28B-positive tumors in fish aligned to the one previously described for human neuroblastomas. We then studied the molecular consequences of enforced short-term and long-term overexpression of the *LIN28B* gene in vitro in NCC-derived neuroblastoma cells. We could distinguish the short-term and long-term effects of *LIN28B* overexpression as respectively *let-7a*-dependent and *let-7a*-independent, sustaining previous findings [39]. Moreover, the LIN28B-driven acquisition of migratory and invasive properties was accompanied by substantial morphological changes and the increase of several mesenchymal markers, sustaining *LIN28B* as a promoter of EMT. During normal embryonic development, NCC undergo EMT and the subsequent migration is largely dependent on the cell-ECM crosstalk. Integrins are composed of diverse heterodimeric transmembrane receptors transducing the signals bidirectionally and regulating cell adhesion, migration, and invasion [40]. In our study, we identified a significant increase of two integrins, ITGA5 and ITGA6, upon long-term *LIN28B* overexpression. The importance of ITGA6 in inducing metastasis has been reported in several cancer types diagnosed in adults [41, 42], whereas in neuroblastoma, its involvement in cell dissemination was not previously described. Conversely, ITGA5 induction has been recently associated with a metastatic neuroblastoma phenotype [43]. Consistent with previous findings, our results highlight the importance of integrin-mediated pro-metastatic behavior in *LIN28B*-overexpressing neuroblastoma cells. They also sustain the role of LIN28B in facilitating a dynamic remodeling of cell adhesion proteins [44]. The recruitment of FA clusters on the plasma membrane of *LIN28B*-overexpressing cells implies their value for sustaining the migratory properties of tumor cells. In this scenario, the activation of downstream pathways at first

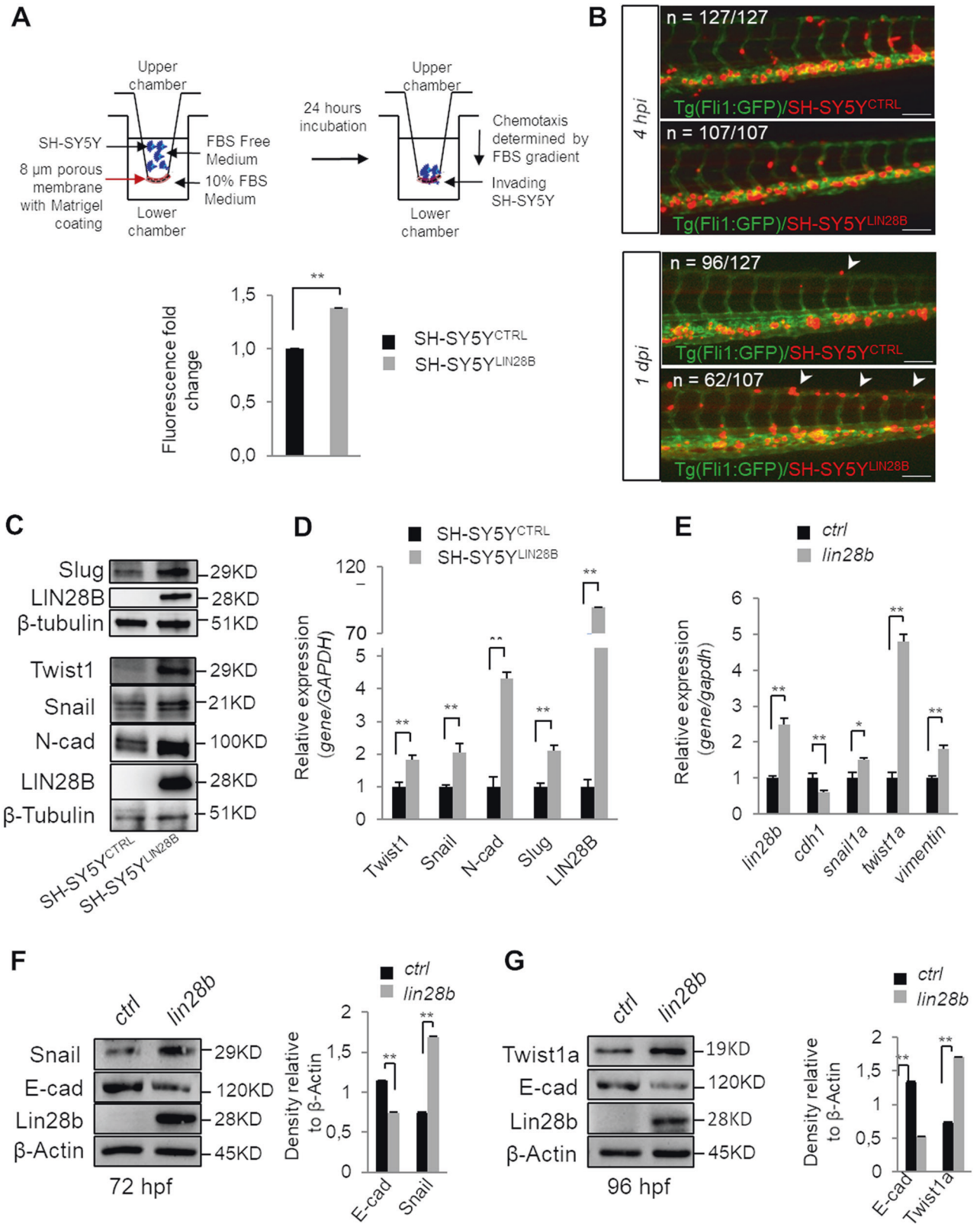

involved the PI3K/AKT and Src kinases, followed by a delayed ERK engagement. All of them were described along with a shift toward more motile phenotypes and a favored FA formation [45]. These results imply that *LIN28B* overexpression promotes mesenchymal-like phenotypes whose motility is allowed by the Integrin/FAK axis and

◀ **Fig. 5** LIN28B activates EMT in neuroblastoma cells and increases their invasive potential in vivo. **a** The assessment of transwell migration was determined 24 h after seeding the SH-SY5Y^{CTRL} and SH-SY5Y^{LIN28B} cells pretreated with doxycycline for 7 days. The quantification of migration was determined by measuring the mean fluorescence intensity, and the results are presented on the histogram. $^{**}p < 0.01$. **b** Fluorescent microscopy images of the trunk region of the *Tg (fli1:GFP)* zebrafish embryos with marked vessels (green) injected at 48 hpf with SH-SY5Y^{CTRL} and SH-SY5Y^{LIN28B} cells (red signal) 7 days upon treatment with doxycycline. Visualizations of cells at 4 h post implantation (hpi) and at 1 day post implantation (dpi) are depicted. White arrowheads indicate cells disseminated throughout the trunk vasculature. n = number of animals analyzed. Scale bar: 100 µm. **c** The western blot analysis for the indicated EMT markers on SH-SY5Y^{CTRL} and SH-SY5Y^{LIN28B} upon 7 days of doxycycline. β-Tubulin was used to show equal protein loading. The molecular weights are indicated in Kilodaltons (KD). **d** The overexpression of *LIN28B* for 7 days increased the expression levels of the mesenchymal markers *Twist1*, *Snail*, *N-cadherin*, and *Slug*. *GAPDH* was used as an internal control. $^{**}p < 0.01$. **e** qPCR analysis for the indicated EMT markers in the ctrl and *lin28b*-overexpressing zebrafish embryos at 48 hpf. The results are normalized to the *gapdh* internal control. The error bars represent SEM. $^{**}p < 0.01$. The western blot analysis of 72 hpf (**f**) and 96 hpf (**g**) zebrafish embryos extracts for the indicated EMT markers and Lin28b protein. β-Actin was used as a loading control. The molecular weights are indicated in Kilodaltons (KD). The quantification of the same is shown in the right graph bars. $^{*}p < 0.05$; $^{**}p < 0.01$

dynamic regulation of several intracellular pathways. Moreover, the striking expression of ITGA5/ITGA6 on the SH-SY5Y^{LIN28B} cell membrane may be critical for shaping the interaction between the ECM and tumor cells and, hence, for their motility and invasion capacities. Both characteristics are required for tumor cells' dissemination and metastasis formation. Our findings specify additional roles of LIN28B in the regulation of the interaction between neuroblastoma cells and their surrounding niche. Previous reports affirm the abundance of fibronectin and laminin, high-affinity binding targets of ITGA5 and ITGA6, within the trunk region of the zebrafish embryos [46, 47]. Their neutralization provokes the inhibition of NCC migration, pointing out the relevance of both ECM molecules for the proper function of NCC [47]. Hence, *hLIN28B*-overexpressing zebrafish could allow not only novel understandings of the cell-ECM interactions but may also serve as an in vivo model for evaluating the effects of selective integrin inhibitors in the treatment of metastatic neuroblastoma.

In conclusion, we confirmed the oncogenic potential of *LIN28B* and its association with neuroblastoma's onset in the zebrafish model. We showed a positive correlation between *LIN28B* overexpression and the induction of EMT, a process that led to the cell morphology transformation and increment of invasive traits of tumor cells. We additionally highlighted the complexity of the LIN28B-dependent pathways not necessarily involving *let-7a* miRNA. Further, we described the association between *LIN28B* overexpression and the prometastatic phenotype of neuroblastoma cells. This feature was triggered by activating *ITGA5* and *ITGA6* expression and by the accumulation of corresponding proteins on the cell membrane. Together, our results suggest that LIN28B sustains integrin-mediated cell spreading and migration by facilitating the formation of focal contacts. The two integrins, ITGA5 and ITGA6, could therefore be new molecular markers in prometastatic neuroblastoma. Further investigation on whether they might be potential targets in a group of HR patients remains to be performed.

Materials and methods

Animals

Wild-type (AB/TU) zebrafish [48] and the transgenic line *Tg (sox10:GFP)* [21] were staged and maintained as described previously [49]. All experiments using animal models were approved by the local Ethical Committees and by the Italian Ministry of Health (zebrafish authorization 86/2016-PR; Xenopus authorization 99/2012-A). Xenopus embryos were obtained and staged as described previously [17].

Cell lines

SH-SY5Y cells were purchased from the DSMZ (Germany) and grown in RPMI-1640 (Sigma-Aldrich) with the addition of 2 mM penicillin/streptomycin (Gibco), 2 mM L-glutamine (Gibco), and 10% fetal bovine serum (FBS; Gibco). Cell line genotyping was conducted prior to the analyses.

SH-SY5Y^{CTRL} and doxycycline-inducible SH-SY5Y-^{LIN28B} cell lines were obtained by a lentiviral infection; pLenti CMV CTRL Blast plasmid (Addgene #17492) and modified pLenti CMV/TO GFP Puro plasmid (GFP was replaced by *LIN28B* ORF, Addgene, #17481) were used. Lentiviral particles were produced by co-transfecting either the CTRL or *LIN28B* plasmids with the packaging vector psPAX2 (Addgene #12260) and the envelope plasmid pMD2.G (Addgene #12259) into HEK-293T cells (ICLC) in the Opti-MEM culture medium (Gibco) with 1 mg/ml polyethylenimine (Sigma-Aldrich). The cells stably expressing the TetR control gene (SH-SY5Y^{CTRL}) were grown in 7 µg/ml of Blasticidin-S HCl (Gibco) enriched selecting medium. A population of SH-SY5Y^{LIN28B} cells was generated upon growth in 2 µg/ml of puromycin (Gibco) enriched selective medium.

Capped mRNA overexpression

The SP6 Message machine kit (Ambion) was used to transcribe synthetic capped RNA. Zebrafish embryos

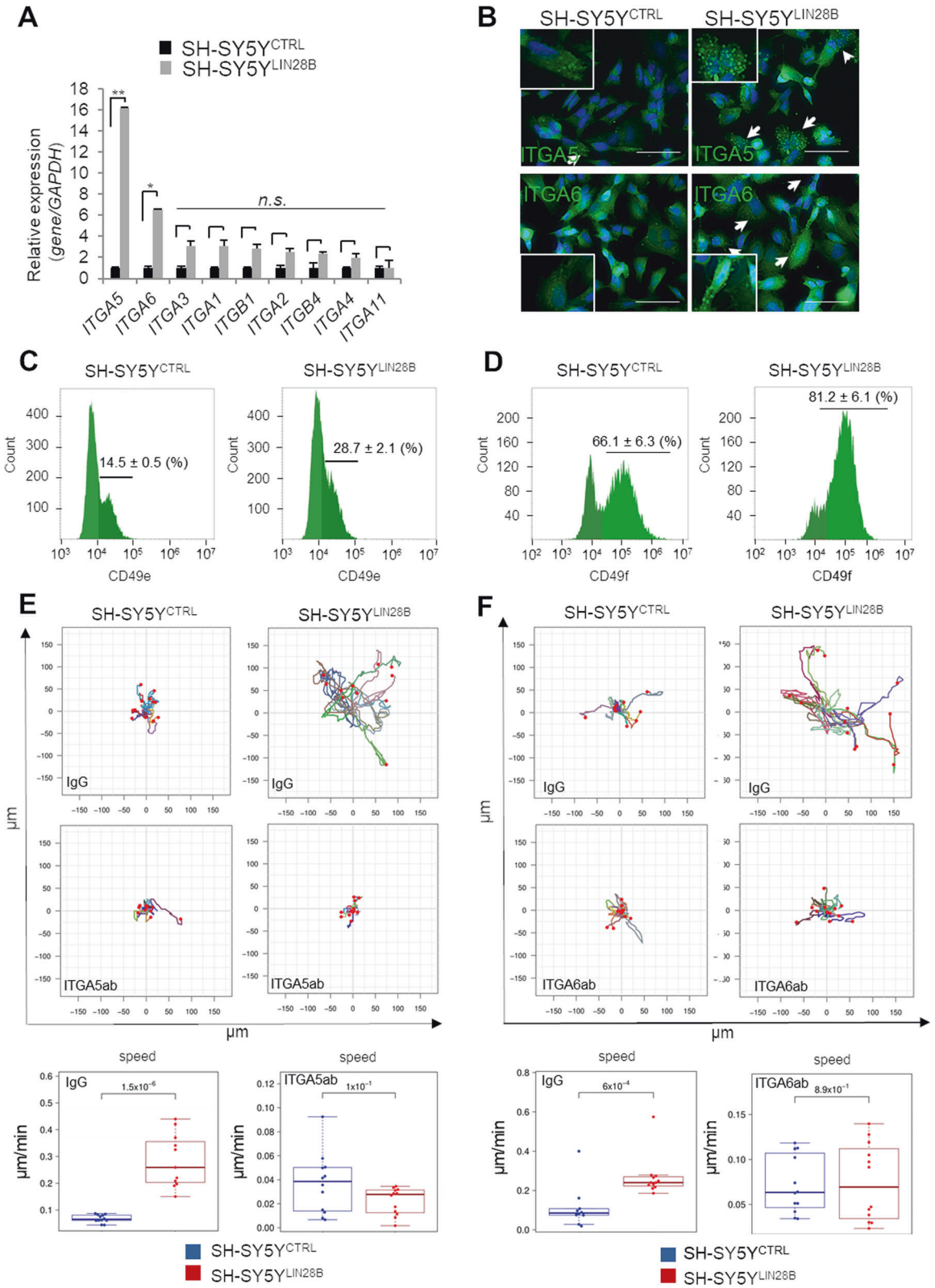

were injected with 50–100 pg of *lin28b* or *GFP* mRNA at the 1–2-cell stage. Injected embryos were raised from 16 h post fertilization (hpf) to 6 days post fertilization (dpf) and fixed with 4% paraformaldehyde for further analysis. Xenopus embryos were injected with *lin28b* or *GFP* mRNA in one blastomere at the four-cell stage, and then fixed with 4% paraformaldehyde for further analysis.

◀ **Fig. 6** Ectopic expression of *LIN28B* triggers integrin expression and increases cell motility potential. **a** qPCR analysis for *ITGAs (ITGA1-6, 11) and ITGBs (ITGB1, 4)* upon 7 days of *LIN28B* overexpression. *GAPDH* was used as an internal control gene. *n.s.*: $*p < 0.05$; $**p < 0.01$. **b** Immunofluorescence on SH-SY5Y^{CTRL} and SH-SY5Y^{LIN28B} cells upon 7 days of doxycycline administration for ITGA5 (green, upper panel) and ITGA6 (lower panel) protein deposition (white arrows). The nuclei were counterstained with DAPI (blue). Scale bar: 50 µm. Insets correspond to higher magnification of the ITGA5/6-positive cells. The flow cytometry profile of SH-SY5Y^{CTRL} and SH-SY5Y^{LIN28B} cells over 7 days of doxycycline administration, showing **c** ITGA5-positive (CD49e, $p = 0.05$, left panel) and **d** ITGA6-positive (CD49f, right panel, $p = 0.04$) cells. **e** The cell motility tracks of SH-SY5Y^{CTRL} and SH-SY5Y^{LIN28B} cells treated with doxycycline for 7 days and incubated with a non-neutralizing IgG control antibody or with the blocking antibody (ab) against ITGA5 (ITGA5ab; 12 cells tracked) prior to the time-lapse imaging. The red dots indicate the final position of the cell migration paths. The corresponding average cell speeds of SH-SY5Y^{CTRL} and SH-SY5Y^{LIN28B} are depicted in the box plots. IgG plot: $p = 3.1 \times 10^{-6}$; ITGA5 plot: $p = 1 \times 10^{-1}$. **f** The cell motility tracks of SH-SY5Y^{CTRL} and SH-SY5Y^{LIN28B} cells treated with doxycycline for 7 days and incubated with a nonneutralizing IgG control antibody or the blocking antibody (ab) against ITGA6 (ITGA6ab; 12 cells tracked) prior to the time-lapse imaging. The red dots indicate the final position of the cell migration paths. The corresponding average cell speeds of SH-SY5Y^{CTRL} and SH-SY5Y^{LIN28B} are depicted as box plots. IgG plot: $p = 6 \times 10^{-4}$; ITGA6 plot: $p = 8.9 \times 10^{-1}$

Constructs and probes

The pCS2^{+}-mCherry construct was a kind gift of Dr Enrico Moro (University of Padua). The pCS2^{+}-GFP was generated from the pME-GFP construct from the Multisite Gateway-based construction kit (Tol2Kit) [50]. Zebrafish *lin28b* cDNAs were obtained by PCR and cloned into the pCS2^{+} vector. The pcDNA3-FLAG-*LIN28B* construct used for the doxycycline-inducible SH-SY5Y cell line was a kind gift from Narry Kim (Addgene plasmid #51373). The following antisense RNA probes were also generous gifts: *dbh, th* [51], and *zash1a* [52]. The *crestin* probe was generated by amplifying the *zebrafish* ORF from the wild-type whole embryo cDNA, and the PCR product was cloned into the pCR-II-TOPO vector (Invitrogen). Following sequence verification, antisense riboprobes were generated by in vitro transcription with a DIG RNA labeling kit Sp6/T7 (Roche). Antisense riboprobes were also generated following sequence verification through in vitro transcription with a DIG RNA labeling kit Sp6/T7 (Roche). The *dre-let-7a* probe was purchased from EXIQON. The Xenopus pCS2^{+}-*lin28b* plasmid was generated by RT-PCR and fully sequenced. The plasmids used for the preparation of *reptin* and *sox10* antisense RNA probes are described elsewhere [53, 54].

Transgenesis

The 5.2-kb promoter region of the *dβh* gene was PCR amplified from the zebrafish BAC clone CH211-270H11 using the primers dβh-fw (#599): GCG TAC TCC CCC TTT TTA GG and dβh-rev (#600): TGT TGC TTT GTC GTC TTT TGA. The PCR product was cloned into the gateway p5-MCS vector (a kind gift of the Chien lab) using the KpnI/XhoI restriction sites. *LIN28B* was isolated from pcDNA3-Flag-*LIN28B* (Addgene #51373) by BamHI/NotI digestion and cloned into the gateway middle entry vector pENTR1A using the same restriction enzymes. The full transgenesis construct was gateway assembled [50] to generate the pDEST5.2*dβh-LIN28B*-CG2. The embryos were injected with this DNA construct at the one-cell stage and grown to adulthood. Fin clips from the offspring were used for the genotyping of stable integration and the germline transmission of the transgene. The *Tg(dβh:hLIN28B)* was designated as the "*hLIN28B*" transgenic line in this article.

In situ hybridization

Whole-mount RNA in situ hybridization of zebrafish and Xenopus embryos was performed, as previously described [17, 55]. Briefly, fixed embryos were permeabilized with 10 µg/ml of Proteinase K and, after 5 h of preincubation with Hybridization Mix (50% Formamide, 5X SSC, 0.01% Tween-20, 50 µg/ml of heparin, 500 µg/ml of t-RNA), they were incubated with 100 ng/µl of the antisense probe at 65 °C. The second day, embryos were extensively washed and incubated in a Blocking Solution (2% sheep serum, 2 mg/ml of BSA in PBS/0.1% Tween-20) for 2 h, followed by the addition of the Anti-Digoxigenin antibody (Anti-Digoxigenin-AP Fab fragment, Roche), diluted 1:3000. The embryos were washed several times in PBTw, followed by the incubation with the Staining Solution containing NBT/BCIP (Roche). Stained embryos were sectioned and mounted in 80% glycerol, and images were acquired with a Carl Zeiss Axio microscope.

Immunofluorescence

Immunofluorescence of whole zebrafish embryos was performed essentially as described [56]. Fixed embryos were permeabilized in cold acetone for 7 min at −20 °C, followed by three washes in PBTx (1% Triton X-100 in 1× PBS) for 5 min at RT in agitation. The embryos were blocked in 3% goat serum diluted in PBTx for 1 h in agitation, and primary antibodies were then added overnight at 4 °C. The embryos were washed three times in PBTx for 10 min and incubated with secondary antibodies in 5% goat serum/PBTx in the dark for 3 h. Lastly, the embryos were washed two times in PBTx for 10 min and transferred in low melting 1.5% agarose (Sigma-Aldrich) and mounted in slides, and images were acquired with a Carl Zeiss Axio microscope and a

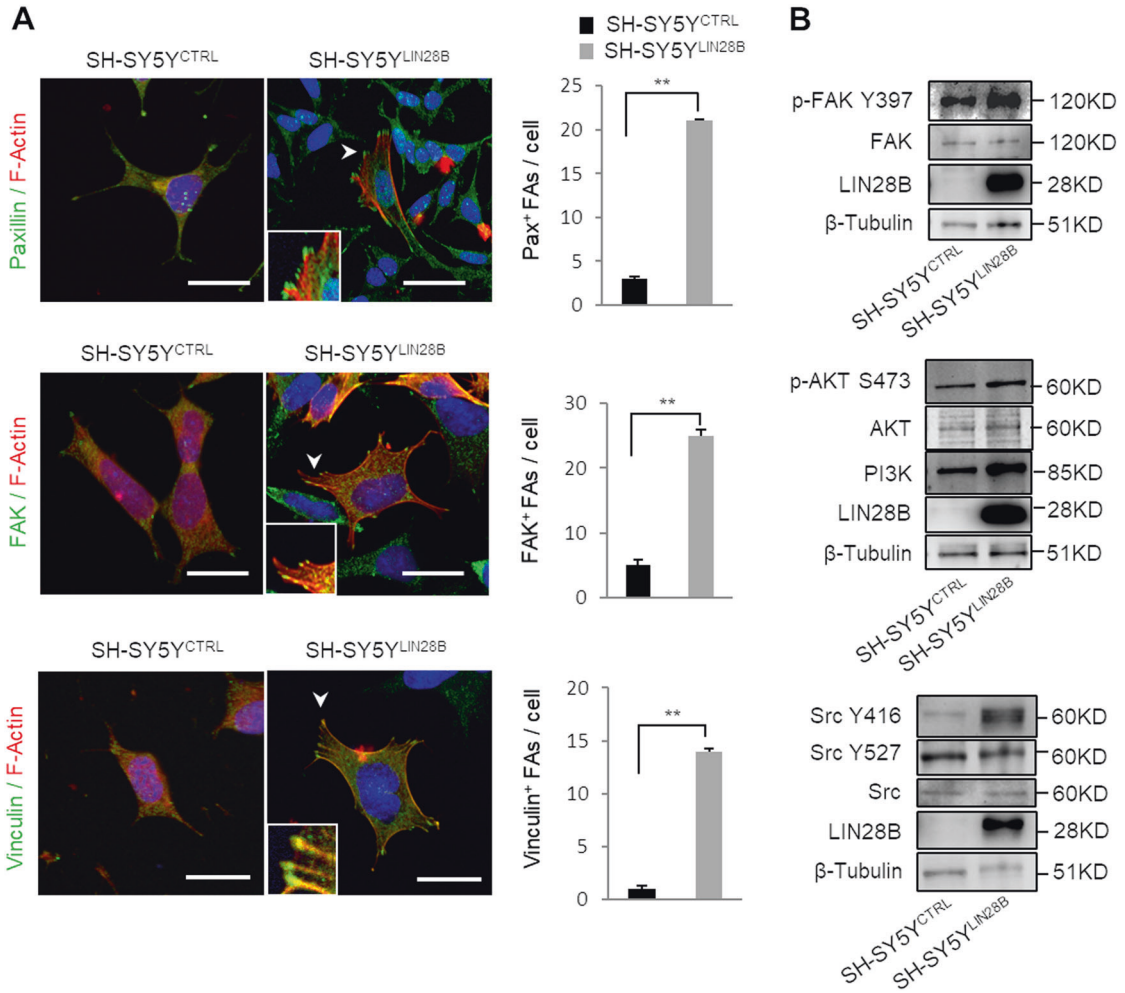

Fig. 7 Ectopic expression of *LIN28B* triggers focal adhesion reorganization and activation of integrin/FAK-related signaling pathway. (**a**) The immunostaining of the focal adhesion (FA) associated adapter proteins Paxillin, FAK, and Vinculin (green) in combination with Phalloidin (F-Actin, red) is presented. Local redistribution of the proteins in the FAs is indicated by white arrowheads and evidenced as insets. The nuclei were counterstained with DAPI (blue). FAs of 5 cells within 3 random fields were counted, and data were presented as mean ± SEM from 3 independent experiments. $^{**}p < 0.01$. (**b**) The Western blot analysis for the indicated markers on SH-SY5Y^{CTRL} and SH-SY5Y^{LIN28B} upon 7 days of doxycycline administration. An antibody against β-Tubulin was used as a loading control. The molecular weights are indicated in Kilodaltons (KD)

Leica TCS-SP5-II confocal microscope. Primary and secondary antibodies are listed in Supplementary Table S1.

SH-SY5Y cells were fixed using 4% PFA in PBS for 15 min before permeabilization with 0.1% Triton X-100 diluted in PBS. To reduce the background fluorescence, the coverslips were blocked in 3% BSA prepared in PBS for 1 h at room temperature. Cells were stained with phalloidin-TRITC, ITGA5, and ITGA6 antibodies. The cells in Fig. S5C were incubated with 3% BSA without cell permeabilization. The proteins were visualized with a Zeiss LSM 800 confocal microscope. For Paxillin, FAK, and Vinculin staining, the coverslips were fixed and permeabilized as previously described. The coverslips were subsequently treated with primary antibodies for 1 h and after PBS washing with a secondary antibody in a dark humid chamber for 45 min. The coverslips were subsequently mounted on glass slides and observed by confocal microscopy (Zeiss LSM 800 confocal microscope). The number of FAs per cell was assessed using ImageJ software.

Western blot

Zebrafish-derived proteins were extracted from pools of 30 embryos through mechanical desegregation in Lysis Buffer (Tissue Extraction Reagent I, Life Technologies) supplemented with 1% Protease/Phosphatase Inhibitor Cocktail (Sigma-Aldrich). The proteins from neuroblastoma cells were extracted with commercially available lysis buffer (Biosource International) from the samples pre-treated with doxycycline, as described previously [57].

Samples were centrifuged at 14,000 × *g* for 5 min at 4 °C, and the protein concentration was determined using the

bicinchoninic assay (BCA) method (Pierce BCA Protein Assay Kit, Thermo Scientific). A total amount of 50 µg (zebrafish) and 20 µg (cell lines) of proteins were loaded in the Criterion™ TGX Stain-Free™ Precast Gels 4–20% (Bio-Rad), and then transferred on the nitrocellulose membrane (Midi-size LF PVDF Membrane, TransBlot®-Turbo™, Bio-Rad, activated in 100% Methanol) through a semidry transfer with the Trans-Blot® TurboTM Transfer System (Bio-Rad). Membranes were blocked with Tropix® I-BLOCK (Thermo Fisher Scientific) for 2 h, followed by incubation with primary antibodies at 4 °C. The membranes were washed and incubated with secondary antibodies. Uvitec Cambridge was used for chemiluminescence detection, covering the membrane with ECL (ECL SelectTM Western Blotting Detection Reagent, GE Healthcare). The primary and secondary antibodies are listed in Supplementary Table S1.

EdU proliferation and TUNEL cell death assays

A proliferation assay was performed using a commercial kit, EdU-Click 488, as recommended by the manufacturer (Baseclick). Briefly, three independent pools of 15 living embryos were collected in microcentrifuge tubes, and 1 mM EdU was added, followed by incubation on ice for a variable time depending on their developmental stage. The embryos were washed with cold E3 medium on ice and then incubated for 30 min at 28.5 °C. After that, embryos were fixed with 4% paraformaldehyde for 2 h and permeabilized in 10 µg/ml Proteinase K. To detect proliferating cells, embryos were incubated in the Reaction Cocktail containing 10 mM of Dye Azide for 3 h. In following, the embryos were used for the coupled immunostainings to detect the SCG or the NCC. Cell death assay was performed using a commercial kit, Click-iT Plus TUNEL Assay, following manufacturer instruction (Life Technologies). Fixed embryos were permeabilized with 10 µg/ml Proteinase K and subsequently incubated with an Equilibration Buffer (TdT reaction buffer) for 1 h. Next, the embryos were incubated with the TdT enzyme for 90 min at 37 °C and then with the Reaction Cocktail for 30 min at 37 °C. The embryos were fixed again in 4% paraformaldehyde for 30 min, and the immunofluorescence with the anti-GFP antibody was then performed (see Supplementary Table S1). The embryos were then mounted in 3% methylcellulose, and images were acquired through a Zeiss LSM 800 confocal microscope.

Fluorescent cell labeling, embryo preparation, and tumor cell implantation

After 7 days of doxycyclin administration, SH-SY5Y^{CTRL} and SH-SY5Y^{LIN28B} cells were labeled with the Vybrant® DiI Cell-Labeling Solution (Invitrogen) according to the manufacturer's instructions. The dechorionized (2 dpf) zebrafish embryos were anaesthetized with 0.003% tricaine (Sigma-Aldrich) and positioned on a 10 cm Petri dish coated with 3% agarose. Approximately 200 cells were injected within the duct of Cuvier of the anesthetized *Tg (fli1:GFP)* embryos using borosilicate glass capillary needles (OD/ID: 1.0/0.75 mm, WPI), a Pneumatic Picopump, and a micromanipulator (WPI). After implantation, zebrafish embryos were maintained at 33 °C. Embryos showing less than 30–40 cells after 4 h post injection were discarded from the analysis. At least 30 embryos per group were analyzed from three independent experiments. The embryos were live photographed using a Nikon C2 H600L confocal microscope (×20 water dipping objective).

Time-lapse

Tg(sox10:GFP) embryos were injected with *LIN28B* mRNA and allowed to develop for 19-20 hpf. Anesthetized embryos were embedded in 1.5% agar, mounted in a heated chamber, and imaged with a Zeiss Axio Observer microscope for live cell imaging for 8 h. Quantification of displacement was measured in a 40 µm Z-stack, tracked using Fiji software. The quantification of the percentage of the migrated distance relative to Fig. 3b was the measurement of the straight-line distance from the first position (neural tube) to the last position labeled with *crestin* riboprobe, with a higher number indicative of more distance between the first and last point. Statistical analysis was conducted in Excel followed by a two-tailed Student's *t*-test. Neuroblastoma cells were analyzed in a 37 °C heated chamber with 5% CO_2. Cell motility was captured over a 12-h period at 10-min intervals, and tracks were recorded using the Fiji "manual tracking" plug-in. For functional integrin blocking, the attached cells were preincubated for 30 min before migration analysis either with 10 µg/ml of mouse anti-human-ITGA6 or mouse anti-human-ITGA5 antibodies in 24-well plates (see Supplementary Table S1). The appropriate IgG antibodies (Mouse IgG2b, Millipore; Mouse IgG1, Santa Cruz Biotechnology) were used as negative controls. Cell motility was captured over a 12-h period at 10-min intervals.

The Wilcoxon test was used to assess the *p*-values quantifying the significance of the differences. All statistical analyses were performed using the R statistical software "stats" package.

Flow cytometric analyses

Zebrafish single-NCC were obtained from the pool of 40 embryos. *Tg(sox10:GFP)* and wild-type zebrafish embryos were dissected to remove the head and washed, and the tails

were mechanically desegregated by constant pipetting in Hanks' buffer (EMD Millipore Corporation). Single-NCC were obtained using Trypsin-EDTA (EMD Millipore Corporation) and Collagenase/Dispase (Sigma-Aldrich). After resuspending the NCC in Hanks' buffer, analyses were performed through Cytomics FC 500 (Beckman Coulter). Wild-type uninjected embryos were used as blanks.

SH-SY5Y^{CTRL} and SH-SY5Y^{LIN28B} cells ($0.3–0.5 \times 10^6$ cells) were incubated with PeCy5 anti-human CD49f (ITGA6, Becton Dickinson) and analyzed using a CytoFLEX Flow cytometer (Beckman Coulter). The percentage of CD49e (ITGA5) positive cells was validated upon coupled primary (1 µg) and secondary antibody labeling (see Supplementary Table S1). The percentage of CD49e- and CD49f-positive cells in both SH-SY5Y^{CTRL} and SH-SY5Y^{LIN28B} cells were considered by setting an appropriate gate on the living cell population (Propidium iodide negative, 10 mg/ml, Roche). Unlabeled cells for each line were first acquired to ensure labeling specificity.

Colony formation assay

Two thousand cells were seeded in a 24-well plate using a MethoCult semisolid medium (Stemcell Technologies) and were grown for 2 weeks. Colonies (foci) were visualized after incubation with MTT. The total colony number was counted under a light microscope in ten random fields and determined by Fiji software.

Transwell migration assay

SH-SY5Y^{CTRL} and SH-SY5Y^{LIN28B} cells were seeded onto inserts without Matrigel (BD Biosciences) in a serum-free medium. Inserts were placed into wells containing a medium supplemented with 10% FBS. After 24 h, the cells on the upper surface of the filters were removed, and the inserts were stained with Hoechst (Sigma-Aldrich) and cristal violet. The numbers of migrated cells were counted under a light and a fluorescent microscope in ten random fields. Using Fiji software, the number of migrated cells per image was determined.

Matrigel invasion assay

SH-SY5Y^{CTRL} and SH-SY5Y^{LIN28B} cells (5×10^4) were seeded onto matrigel-coated transwell chambers (BD Biosciences) with an 8-µm pore size filter using an FBS gradient (0–10%) from the top to the bottom well. After 24 h of incubation, the filter was removed and washed, and the cells that invaded the lower side of the filter were stained with calcein (Sigma-Aldrich). The absorbance was measured using the VICTOR™ Multilabel Plate Reader (PerkinElmer, Waltham, MA) at 495 nm.

Scratch test

SH-SY5Y^{CTRL} and SH-SY5Y^{LIN28B} cells (3×10^4) were plated within each of the two-cell culture reservoirs separated by a 500-µm-thick silicone wall (IBIDI, Milano, Italy). The day after, the silicone insert was removed and the cells were allowed to grow for another 48–72 h. Images were taken every 24 h by a Nikon Eclipse TS100 microscope (Nikon Eclipse TS100, Southern Micro Instruments, Marietta, GA) equipped with a Nikon Coolpix camera. Wound healing was analyzed by Fiji software for each time point.

RNA analysis

Total RNA was extracted from the pool of 30 embryos or cell pellets using TRIzol Reagent (Invitrogen), and 2 µg of RNA were used for cDNA synthesis using Super Script II (Invitrogen), according to the manufacturer's recommendations. The cDNA was subjected to PCR reaction using the AmpliTaq DNA polymerase (Thermo Fisher Scientific).

The expression of *lin28b*, *cdh1, snail1a, twist1a*, and *vimentin* transcripts was analyzed by real-time quantitative PCR (qPCR) using the SYBR Green PCR Master Mix (Applied Biosystems) in an Applied Biosystems 7900HT Fast Real-Time PCR System. Primer dissociation curves were checked in each run to ensure primer specificity in human and zebrafish mRNA. The expression of *gapdh* was used as a normalizer in each sample, and triplicate PCR reactions were carried out. Primers were designed using the Primer 3 software and are listed in Supplementary Table S2.

MicroRNA (miRNA) measurement by qPCR

Total RNA was isolated from SH-SY5Y^{CTRL} and SH-SY5Y^{LIN28B} as well as from the pool of 30 embryos using the Qiazol Lysis Reagent (Qiagen), and 10 ng of total RNA solution were reverse transcribed using the miScript II RT Kit (Qiagen). Specific miRNA levels were quantified by qPCR using the TAQMAN microRNA Assay (Life Technologies) for *hsa-miR-let-7a* together with the universal RT primer, according to the manufacturer's protocol. The relative quantities of the miRNAs were calculated using the Cq value after normalization to control the miRNA (*RUN6B*).

Quantification and statistical analysis

All data were expressed as the mean ± SEM of experimental triplicates. Statistical significance was determined using the Student's *t*-test; $p < 0.05$ was considered significant and was marked with an asterisk (*) on the graphs while $p < 0.01$ was marked with two asterisks (**).

The statistical significance of the cells' migratory differences related to time-lapse experiments was calculated using the Wilcoxon test (from the R software 'stats' package), and box plots (using the R software "stats" package) reported the quartile distribution of related variables.

Acknowledgements The authors would like to thank the Fondazione Italiana per la Lotta al Neuroblastoma and the Fondazione Veronesi (FUV) for their support. We also thank Elisa Lidron (University of Padua), Valentina Tonelotto (University of Padua), and Claudia Grigoletto (University of Trieste) for their excellent technical assistance.

Funding This work was supported by funds from Fondazione Italiana per la Lotta al Neuroblastoma and from the Fondazione Istituto di Ricerca Pediatrica Città della Speranza (project number *19_07IRP*). Corallo Diana was supported by a Fondazione Veronesi (FUV) Post-doctoral fellowship.

Compliance with ethical standards

Conflict of interest The authors declare that they have no conflict of interest.

Publisher's note Springer Nature remains neutral with regard to jurisdictional claims in published maps and institutional affiliations.

References

1. Kerosuo L, Bronner-Fraser M. What is bad in cancer is good in the embryo: importance of EMT in neural crest development. Semin Cell Dev Biol. 2012;3:320–32.
2. Anderson DJ, Carnahan JF, Michelsohn A, Patterson PH. Antibody markers identify a common progenitor to sympathetic neurons and chromaffin cells in vivo and reveal the timing of commitment to neuronal differentiation in the sympathoadrenal lineage. J Neurosci. 1991;11:3507–19.
3. Kulesa PM, Gammill LS. Neural crest migration: patterns, phases and signals. Dev Biol. 2010;2:566–8.
4. King CE, Wang L, Winograd R, Madison BB, Mongroo PS, Johnstone CN, et al. LIN28B fosters colon cancer migration, invasion and transformation through let-7-dependent and-independent mechanisms. Oncogene. 2011;30:4185–93.
5. Xiong H, Zhao W, Wang J, Seifer BJ, Ye C, Chen Y, et al. Oncogenic mechanisms of Lin28 in breast cancer: new functions and therapeutic opportunities. Oncotarget. 2017;8:25721–35.
6. Hamano R, Miyata H, Yamasaki M, Sugimura K, Tanaka K, Kurokawa Y, et al. High expression of Lin28 is associated with tumour aggressiveness and poor prognosis of patients in oesophagus cancer. Br J Cancer. 2012;106:1415–23.
7. Molenaar JJ, Domingo-Fernández R, Ebus ME, Lindner S, Koster J, Drabek K, et al. LIN28B induces NB and enhances MYCN levels via let-7 suppression. Nat Genet. 2012;44:1199–206.
8. Luksch R, Castellani MR, Collini P, De Bernardi B, Conte M, Gambini C, et al. NB (Peripheral neuroblastic tumours). Crit Rev Oncol Hematol. 2016;107:163–81.
9. De Preter K, Vandesompele J, Heimann P, Yigit N, Beckman S, Schramm A, et al. Human fetal neuroblast and NB transcriptome analysis confirms neuroblast origin and highlights NB candidate genes. Genome Biol. 2006;7:R84.
10. Shimada H, Ambros IM, Dehner LP, Hata JI, Joshi VV, Roald B, et al. The International NB Pathology Classification (the Shimada system). Cancer. 1999;86:364–72.
11. Cohn SL, Pearson ADJ, London WB, Monclair T, Ambros PF, Brodeur GM, et al. The International NB Risk Group (INRG) classification system: an INRG task force report. J Clin Oncol. 2009;27:289–97.
12. Pugh TJ, Morozova O, Attiyeh EF, Asgharzadeh S, Wei JS, Auclair D, et al. The genetic landscape of high-risk NB. Nat Genet. 2013;45:279–84.
13. Moss EG, Lee RC, Ambros V. The cold shock domain protein LIN-28 controls developmental timing in C. elegans and is regulated by the lin-4 RNA. Cell. 1997;88:637–46.
14. Tsialikas J, Romer-Seibert J. LIN28: roles and regulation in development and beyond. Development. 2015;142:2397–404.
15. Zhou J, Ng SB, Chng WJ. LIN28/LIN28B: an emerging oncogenic driver in cancer stem cells. Int J Biochem Cell Biol. 2013;5:973–8.
16. Helsmoortel HH, Bresolin S, Lammens T, Cavé H, Noellke P, Caye A, et al. LIN28B overexpression defines a novel fetal-like subgroup of juvenile myelomonocytic leukemia. Blood. 2016;127:1163–72.
17. Guillemot F, Lo LC, Johnson JE, Auerbach A, Anderson DJ, Joyner AL. Mammalian achaete-scute homolog 1 is required for the early development of olfactory and autonomic neurons. Cell. 1993;75:463–76.
18. Naef V, Monticelli S, Corsinovi D, Mazzetto MT, Cellerino A, Ori M. The age-regulated zinc finger factor ZNF367 is a new modulator of neuroblast proliferation during embryonic neurogenesis. Sci Rep. 2018;8:11836.
19. Stewart RA, Look AT, Kanki JP, Henion PD. Development of the peripheral sympathetic nervous system in zebrafish. Methods Cell Biol. 2004;76:237–60.
20. Teitelman G, Baker H, Joh TH, Reis DJ. Appearance of catecholamine-synthesizing enzymes during development of rat sympathetic nervous system: Possible role of tissue environment. Proc Natl Acad Sci USA. 1979;76:509–13.
21. Dutton JR, Antonellis A, Carney TJ, Rodrigues FSLM, Pavan WJ, Ward A, et al. An evolutionarily conserved intronic region controls the spatiotemporal expression of the transcription factor Sox10. BMC Dev Biol. 2008;8:105.
22. Luo R, An M, Arduini BL, Henion PD. Specific pan-neural crest expression of zebrafish crestin throughout embryonic development. Dev Dyn. 2001;220:169–74.
23. Richards M. The transcriptome profile of human embryonic stem cells as defined by SAGE. Stem Cells. 2004;22:51–64.
24. Kelsh RN, Brand M, Jiang YJ, Heisenberg CP, Lin S, Haffter P, et al. Zebrafish pigmentation mutations and the processes of neural crest development. Development. 1996;123:369–89.
25. Theveneau E, Mayor R. Neural crest delamination and migration: from epithelium-to-mesenchyme transition to collective cell migration. Dev Biol. 2012;336:34–54.
26. Heanue TA, Shepherd IT, Burns AJ. Enteric nervous system development in avian and zebrafish models. Dev Biol. 2016;417:129–38.
27. Yu J, Vodyanik MA, Smuga-Otto K, Antosiewicz-Bourget J, Frane JL, Tian S, et al. Induced pluripotent stem cell lines derived from human somatic cells. Science. 2007;318:1917–20.
28. Mitchison TJ, Cramer LP. Actin-based cell motility and cell locomotion. Cell. 1996;3:371–79.
29. Hood JD, Cheresh DA. Role of integrins in cell invasion and migration. Nat Rev Cancer. 2002;2:91–100.
30. Kragtorp KA, Miller JR. Integrin alpha5 is required for somite rotation and boundary formation in Xenopus. Dev Dyn. 2007;236:2713–20.
31. Julich D, Cobb G, Melo AM, McMillen P, Lawton AK, Mochrie SG, et al. Cross-scale integrin regulation organizes ECM and tissue topology. Dev Cell. 2015;34:33–44.

32. Banning A, Babuke T, Kurrle N, Meister M, Ruonala M, Tikkanen R. Flotillins regulate focal adhesions by interacting with a-actinin and by influencing the activation of focal adhesion kinase. Cells. 2018;7:E28.
33. Owens DW, McLean GW, Wyke AW, Paraskeva C, Parkinson EK, Frame MC, et al. The catalytic activity of the Src family kinases is required to disrupt cadherin-dependent cell–cell contacts. Mol Biol Cell. 2000;11:51–64.
34. Avizienyte E, Fincham VJ, Brunton VG, Frame MG. Src SH3/2 domain-mediated peripheral accumulation of Src and phosphomyosin is linked to deregulation of E-cadherin and the epithelial–mesenchymal transition. Mol Biol Cell. 2004;15: 2794–803.
35. Wang H, Zhao Q, Deng K, Guo X, Xia J. Lin28: an emerging important oncogene connecting several aspects of cancer. Tumour Biol. 2016;37:2841–8.
36. Permuth-Wey J, Kim D, Tsai YY, Lin HY, Chen YA, Barnholtz-Sloan J, et al. LIN28B polymorphisms influence susceptibility to epithelial ovarian cancer. Cancer Res. 2011;71:3896–903.
37. Nguyen LH, Robinton DA, Seligson MT, Wu L, Li L, Rakheja D, et al. LIN28B is sufficient to drive liver cancer and necessary for its maintenance in murine models. Cancer Cell. 2014;26:248–61.
38. Zhu S, Lee JS, Guo F, Shin J, Perez-Atayde AR, Kutok JL, et al. Activated ALK collaborates with MYCN in neuroblastoma pathogenesis. Cancer Cell. 2012;21:362–73.
39. Hennchen M, Stubbusch J, Abarchan-El Makhfi I, Kramer M, Deller T, Pierre-Eugene C, et al. LIN28B and Let-7 in the control of sympathetic neurogenesis and NB development. J Neurosci. 2015;35:16531–44.
40. Kalappurakkal JM, Anilkumarr AA, Patra C, van Zanten TS, Sheetz MP, Mayor S. Integrin mechano-chemical signaling generates plasma membrane nanodomains that promote cell spreading. Cell. 2019;177:1738–56.
41. Laudato S, Patil N, Abba ML, Leupold JH, Benner A, Gaiser T, et al. P53-induced miR-30e-5p inhibits colorectal cancer invasion and metastasis by targeting ITGA6 and ITGB1. Int J Cancer. 2017;141:1879–90.
42. Brooks DLP, Schwab LP, Krutilina R, Parke DN, Sethuraman A, Hoogewijs D, et al. ITGA6 is directly regulated by hypoxia-inducible factors and enriches for cancer stem cell activity and invasion in metastatic breast cancer models. Mol Cancer. 2016;15:26.
43. Zhu S, Zhang X, Weichert-Leahey N, Dong Z, Zhang C, Lopez G, et al. LMO1 synergizes with MYCN to promote NB initiation and metastasis. Cancer Cell. 2017;32:310–23.
44. Kim TH, Kim HI, Soung YH, Shaw LA, Chung J. Integrin (alpha6beta4) signals through Src to increase expression of S100A4, a metastasis promoting factor: implications for cancer cell invasion. Mol Cancer Res. 2009;7:1605–12.
45. Avizienyte E, Frame MC. Src and FAK signalling controls adhesion fate and the epithelial-to-mesenchymal transition. Curr Opin Cell Biol. 2005;17:542–7.
46. Crawford BD, Henry CA, Clason TA, Becker AL, Hille MB. Activity and distribution of paxillin, focal adhesion kinase, and cadherin indicate cooperative roles during zebrafish morphogenesis. Mol Biol Cell. 2003;14:3065–81.
47. Bilozur ME, Hay ED. Neural crest migration in 3D extracellular matrix utilizes laminin, fibronectin, or collagen. Dev Biol. 1988;125:19–33.
48. Westerfield M. The zebrafish book. a guide for the laboratory use of zebrafish (Danio rerio). 3rd ed. Eugene, OR: Univ Oregon Press; 1995.
49. Kimmel CB, Ballard WW, Kimmel SR, Ullmann B, Schilling TF. Stages of embryonic development of the zebrafish. Dev Dyn. 1995;203:253–310.
50. Kwan KM, Fujimoto E, Grabher C, Mangum BD, Hardy ME, Campbell DS, et al. The Tol2kit: a multisite gateway-based construction Kit for Tol2 transposon transgenesis constructs. Dev Dyn. 2007;236:3088–99.
51. Holzschuh J, Barrallo-Gimeno A, Ettl AK, Durr K, Knapik EW, Driever W. Noradrenergic neurons in the zebrafish hindbrain are induced by retinoic acid and require tfap2a for expression of the neurotransmitter phenotype. Development. 2003;130:5741–54.
52. Allende ML, Weinberg ES. The expression pattern of two zebrafish achaete-scute homolog (ash) genes is altered in the embryonic brain of the cyclops mutant. Dev Biol. 1994;166:509–30.
53. Etard C, Gradl D, Kunz M, Eilers M, Wedlich D. Pontin and Reptin regulate cell proliferation in early Xenopus embryos in collaboration with c-Myc and Miz-1. Mech Dev. 2005;122:545–56.
54. Giannetti K, Corsinovi D, Rossino C, Appolloni I, Malatesta P, Ori M. Platelet derived growth factor B gene expression in the Xenopus laevis developing central nervous system. Int J Dev Biol. 2016;60:175–9.
55. Thisse B, Thisse C. In situ hybridization on whole-mount zebrafish embryos and young larvae. Methods Mol Biol. 2014;1211: 53–67.
56. Corallo D, Schiavinato A, Trapani V, Moro E, Argenton F, Bonaldo P. Emilin3 is required for notochord sheath integrity and interacts with Scube2 to regulate notochord-derived Hedgehog signals. Development. 2013;140:4594–601.
57. Aveic S, Corallo D, Porcù E, Pantile M, Boso D, Zanon C, et al. TP-0903 inhibits neuroblastoma cell growth and enhances the sensitivity to conventional chemotherapy. Eur J Pharm. 2018;818: 435–48.